Integrated MEG/EEG and fMRI Model Based on Neural Masses

Abbas Babajani and Hamid Soltanian-Zadeh*, *Senior Member, IEEE*

***Abstract*—We introduce a bottom-up model for integrating electroencephalography (EEG) or magnetoencephalography (MEG) with functional magnetic resonance imaging (fMRI). An extended neural mass model is proposed based on the physiological principles of cortical minicolumns and their connections. The fMRI signal is extracted from the proposed neural mass model by introducing a relationship between the stimulus and the neural activity and using the resultant neural activity as input of the extended Balloon model. The proposed model, validated using simulations, is instrumental in evaluating the upcoming combined methods for simultaneous analysis of MEG/EEG and fMRI.**

***Index Terms*—EEG, fMRI, integrated model, MEG, neural mass.**

I. Introduction

In THE LAST few years, numerous efforts have been directed at multimodal data fusion. Electroencephalography (EEG), magnetoencephalography (MEG), and functional magnetic resonance imaging (fMRI) are innovative functional brain imaging techniques. The spatiotemporal resolution of these techniques is different. EEG and MEG have good temporal resolutions in the order of millisecond, but their spatial resolutions are poor due to ill-posedness of the inverse solution. On the other hand, fMRI has good spatial resolution in the order of millimeter but poor temporal resolution due to the limited rate of change in the hemodynamic response. Since MEG/EEG and fMRI are different views of a common source (neural activity), their integrate analysis should improve the overall spatiotemporal resolution. Several sophisticated methods have been introduced for MEG/EEG and fMRI combined analysis [1]–[4] in order to extract as much information as possible using a data-driven strategy (the authors refer to them as top-down methods).

Although integrated MEG/EEG and fMRI model (bottom-up modeling) is an active area of research, there is limited work about it in the literature [5]. The integrated model proposed by Riera *et al.* [6], [7] is one of the most recent works in this field. They introduce a two-dimensional autoregressive model with exogenous variables to describe the relationships between synaptic activity and hemodynamics. They use a static nonlinear function to describe the electro-vascular coupling through a flow-inducing signal. In this work, a linear filter for step from the stimulus to the synaptic activities is used, while experimental results report a nonlinear relationship between them [8], [9]. Moreover, their assumption about linear relationship between cerebral blood flow (CBF) and blood oxygen level dependent (BOLD) is not generally valid [10].

We propose an integrated model in this paper which is totally different from the integrated model in [7] and does not have the above limitations. The proposed integrated bottom-up model is based on the neural mass model. The neural mass models comprise macro-columns, or even cortical areas, using a few state variables to represent the mean activity of the whole neuronal population. There are several views and methods in neural mass modeling [11]–[17]. We use the Jansen's model [14] as the base of the proposed model. However, the Jansen's model has few parameters and does not have the flexibility to generate various event-related potentials (ERP). As the first contribution of this paper, we extend the Jansen's model and propose an extended neural mass model in a cortical area. The extended neural mass model is based on the physiological principles of cortical minicolumns and their connections. We illustrate that the model is capable to produce various ERP. In another work, David *et al.* in [12] extend the Jansen's model in multiple cortical areas with introducing Bottom-up, Top-down and Lateral connections between them. They use the Jansen's model in each area. We also extend their work using a new model of an area, based on a physiological modeling of the minicolumns with an extended neural mass model.

We use the extended Balloon model (EBM) in the fMRI part of the proposed integrated model. The Balloon model was proposed by Buxton *et al.* [10]. In this model, a model of oxygen exchange is linked to the venous dilation processes due to CBF variations, and the BOLD signal is derived from the total deoxyhemoglobin content within a voxel. In the EBM proposed by Friston *et al.* [18], the Balloon model [10] is used for relating the CBF to the BOLD and a model of CBF autoregulation is added to the Balloon model which is linear and relates the synaptic activity to the CBF. The step from the stimulus to the synaptic activity is not proposed in the EBM which is reported nonlinear in experimental results [7], [8]. We propose a nonlinear model for this step which is in agreement with the experimental results.

The second and main contribution of this paper is a new integrated MEG/EEG and fMRI model based on the neural mass model. Thanks to our extension of the neural mass model, the neural mass model that has so far been used for the MEG/EEG modeling only, has been used here for the first time for the fMRI modeling. The originality of our approach is to suggest a nonlinear relationship between the stimuli and the neural activity using our extended neural mass model. Thus, with the combination of this new neural activity model and the EBM, we obtain

Manuscript received August 1, 2005; revised December 16, 2005. This work was supported in part by a grant from the Research Council of the University of Tehran, Tehran, Iran. *Asterisk indicates corresponding author.*

A. Babajani is with the Control and Intelligent Processing Center of Excellence, Electrical and Computer Engineering Department, University of Tehran, Tehran 14395-515, Iran (e-mail: a.babajani@ece.ut.ac.ir).

*H. Soltanian-Zadeh is with the Radiology Image Analysis Laboratory, Henry Ford Health System, Detroit, MI 48202 USA. He is also with the Control and Intelligent Processing Center of Excellence, Electrical and Computer Engineering Department, University of Tehran, Tehran 14395-515, Iran (e-mail: hamids@rad.hfh.edu; hszadeh@ut.ac.ir).

Digital Object Identifier 10.1109/TBME.2006.873748

an fMRI model that is naturally integrated with an MEG/EEG model. We justify our model of the neural activity by comparing the simulation results with other experimental data. Although we emphasize EEG in the rest of the paper, without loss of generality, the EEG and the ERP can be replaced by the MEG and event-related field (ERF), respectively.

The organization of the paper is as follows. In Section II, the extended neural mass model is presented and then the EEG and the fMRI signals are derived from this model. Section III is dedicated to the analysis of the proposed model by reporting a variety of simulation results. The conclusion is given in Section IV.

II. Proposed Integrated Model

A. Neural Mass Model

1) Jansen's Model: The neural mass model proposed by Jansen and Rit [14] is based on a previous lumped parameter model [15]. A cortical column is modeled by a population of excitatory pyramidal cells, receiving inhibitory feedback from the local interneurons and excitatory input from the stellate cells. The solid box in Fig. 1 shows the Jansen's model with some changes in its arrangement and notations. Each of the neuron populations is modeled by two blocks. The first block transforms the average pulse density of presynaptic input coming to the population of neurons into an average postsynaptic membrane potential (PSP) which can be either excitatory or inhibitory. This block represents a linear transformation with an impulse response. The impulse responses of the excitatory and the inhibitory synapses, shown by "he" and "hi" in Fig. 1, are in the form of

$$h_{e,i}(t) = H_{e,i}\frac{t}{\tau_{e,i}}\exp\left(-\frac{t}{\tau_{e,i}}\right); \quad t \geq 0 \tag{1}$$

where H_e and H_i determine the maximum amplitude of the excitatory and inhibitory PSP, respectively. The parameters τ_e and τ_i are the lumped representation of the sum of time constants of the passive membrane and other spatially distributed delays in the dendritic tree. The values of $H_e = 3.25\,\mathrm{mV}$, $H_i = 22\,\mathrm{mV}$, $\tau_e = 10\,\mathrm{ms}$, and $\tau_i = 20\,\mathrm{ms}$ are physiologically plausible and produce oscillating output in the model [14].

The second block, represented by "S" operator in Fig. 1, transforms the average membrane potential of the population into an average rate of APs fired by the neurons. This instantaneous transformation is described by the sigmoid function. In this paper, we use the following sigmoid function proposed by David *et al.* [12] according to zero resting state for all variables in ERP

$$S(v) = \frac{2e_0}{1+\exp(-rv)} - e_0 \tag{2}$$

where e_0 and r are the parameters that determine the shape of the sigmoid function. The nonlinear relationship between the stimulus and the neural activity in our model stems from the nonlinear behavior of the sigmoid function. The four constants γ_i control the strength of the intrinsic connections and represent the total number of synapses in each subpopulation. Using anatomical information from the literature, as described in [14], the relative values of these constants are fixed:$\gamma_2 = 0.8\gamma_1$, $\gamma_3 = \gamma_4 = 0.25\gamma_1$. $x_1(\mathrm{t})$, $x_2(\mathrm{t})$, $x_3(\mathrm{t})$, and $x_4(\mathrm{t})$ in Fig. 1 show overall PSP of different cells. $x_1(\mathrm{t})$ and $x_4(\mathrm{t})$ show overall PSPs of the stellate cells and interneurons, respectively. $x_2(\mathrm{t})$ and $x_3(\mathrm{t})$ show the excitatory and inhibitory overall PSPs of the pyramidal cells, respectively. The MEG/EEG signal is modeled by the PSP of the pyramidal cells as $y(\mathrm{t}) = x_2(\mathrm{t}) - x_3(\mathrm{t})$.

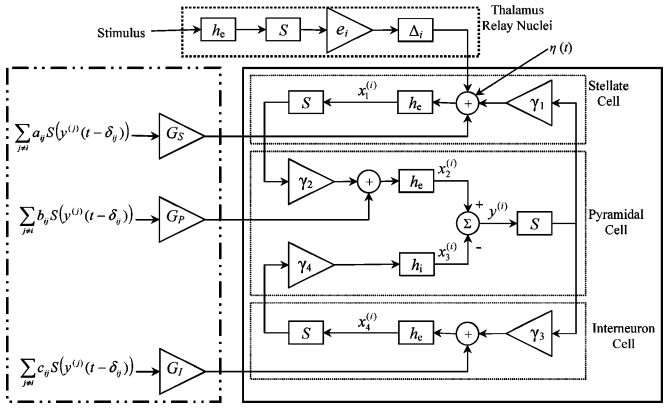

Fig. 1. An illustration of the proposed extended neural mass model for the ith minicolumn. The solid box shows the classical Jansen's model. The left dash-dot box illustrates contributions of the neighboring minicolumns to the ith minicolumn. The MEG/EEG signal is related to $y^{(i)}$. h_{e} and h_{i} are impulse responses of the excitatory and the inhibitory synapses according to (1). $S(.)$ is the sigmoid function. $x_k^{(i)}$ shows overall PSP of different cell populations. The four constants γ_{i} represent the total number of synapses in each subpopulation. G_S, G_P, and G_I represent the influence of the neighboring minicolumns on the stellate cells, pyramidal cells and interneurons, respectively. a_{ij}, b_{ij}, and c_{ij} represent the strength of the connections of different cell populations between the ith and the jth minicolumns. δ_{ij} is the propagation delay between minicolumns i and j. e_i represents strength of the afferent input to the ith minicolumn. Δ_i is the propagation delay between external stimulus $(\mathrm{Stim}(.))$ and cortical columns. $\eta(t)$ is physiological noise.

2) Proposed Extended Neural Mass Model: The minicolumn is the basic unit of the mature neocortex which is a narrow chain of neurons extending vertically across the cellular layers II-VI. Each minicolumn in primates contains roughly 80–100 neurons [19]. The width of each minicolumn is 50 $\mu\mathrm{m}$ and the mean value for intercolumnar distance is 80 $\mu\mathrm{m}$ [20]. There are three basic cell types in minicolumns: the stellate cells, the local inhibitory interneurons and the pyramidal cells; the axon of the two former ones spread vertically in their minicolumn without any considerable outputs to the neighboring minicolumns. The output of a minicolumn is mainly derived from its pyramidal cells and so all cell types in a minicolumn receive input from pyramidal cells of the neighboring minicolumns. The stellate cells also receive afferent thalamic input [20].

The thalamo-cortical connections have been the focus of several modeling studies [21], [22], but the thalamic nuclei are not included in the Jansen's model. We add the thalamo-cortical feed forward connection to the Jansen's model as shown in Fig. 1. The thalamus is part of thalamo-cortical loops, which means that it sends and receives information to and from the cortex. The feedback from the cortex to thalamus is particularly important in spontaneous activity and it is tightly linked to the frequency of EEG oscillations. In the event-related activity, the feedback from the cortex to the thalamus is much weaker than the feedforward connection between the thalamus and the cortex [22]. For this reason, and for simplicity, we do not include the feedback in the proposed model. However, it can be included for applications in which the role of this feedback is important.

The interaction between different neurons in a minicolumn can be explained by the Jansen's model. According to the hierarchical structure of the cell assemblies, we extend the Jansen model to a cortical area which contains several minicolumns. The proposed extended neural mass model is based on physiological principles explained in the previous paragraph and shown in Fig. 1. As proposed in [12], the model can be further extended by considering connections between multiple areas. For the sake of clarify, in the sequel we do not consider the interarea connections and focus on a single area to present our extended model.

Fig. 1 shows different parts of the proposed extended neural mass model in ith minicolumn. Solid box in Fig. 1 represents three population cell types (stellate cell, pyramidal cell, and inhibitory interneuron), which model the neural activation of each minicolumn in the proposed model. Stellate cell receives an input from pyramidal cell in the same minicolumn, inputs from pyramidal cells in neighboring minicolumns, afferent thalamic input and physiological noise. The physiological noise, represented by $\eta(t)$ in Fig. 1, models all inputs to the minicolumn that do not have correlations with the external stimulus and can be considered as white Gaussian noise. Stellate cells receive input from the external stimulus through the thalamic relay nuclei, which is shown with dotted block at the top of Fig. 1. The parameter e_i shows the stimulus gain, which affects the ith minicolumn and it will be modeled with a Gaussian kernel. Δ_i is the propagation delay between the external stimulus and the ith minicolumn.

The synapses of the stellate cell receive pulses, which are generated by pyramidal cell in the same minicolumn through the gain parameter γ_1. γ_1 represents the relative number of synapses of the stellate cell subpopulation. Overall synaptic activities of the stellate cells in the ith minicolumn are represented by $x_1^{(i)}$. The effect of neighboring minicolumn on the ith minicolumn is shown with the dash-dot block in the left side of Fig. 1. a_{ij} and δ_{ij} show strength and delay of the input to the stellate cell in the ith minicolumn from the pyramidal call in the jth minicolumn ($S(y^{(j)})$), respectively. $S(.)$ is the sigmoid operator according to (2). G_s is a global gain that represents the overall effects of the neighboring minicolumns on the input of the stellate cell in each minicolumn.

Pyramidal cell in Fig. 1 has two parts that model the excitatory and inhibitory synapse populations in this cell. Inhibitory synapses of the pyramidal cell receive input from inhibitory interneurons of the same minicolumn. Excitatory synapses receive input from the stellate cells of the same minicolumn and inputs from the pyramidal cells of the neighboring minicolumns. γ_2 and γ_4 represent the relative number of excitatory and inhibitory synapses of the pyramidal cell, respectively. Overall excitatory and inhibitory synaptic activities of the pyramidal cells in the ith minicolumn are represented by $x_2^{(i)}$ and $x_3^{(i)}$, respectively. b_{ij} shows strength of the input to the excitatory synapses of the pyramidal cells in the ith minicolumn from the pyramidal cells in the jth minicolumn. G_p represents the gain of the overall effects of the neighboring minicolumns on the input of the excitatory synapses of the pyramidal cells in each minicolumn. $y^{(i)}$ shows the overall synaptic activities of the pyramidal cells and generate the MEG and EEG signals. In the proposed model, $S(y^{(i)})$ is the AP generated by the pyramidal cells and is the output of the ith minicolumn to other minicolumns.

The inhibitory interneuron in Fig. 1 receives an input from the pyramidal cells of same minicolumn and other inputs from the pyramidal cells of the neighboring minicolumns. γ_3 and $x_4^{(i)}$ are the relative number of the interneuron synapses and the overall interneurons synaptic activities in the ith minicolumn, respectively. c_{ij} shows strength of the input to the interneuron in the ith minicolumn from the pyramidal cells in the jth minicolumn. G_I represents gain of the overall effects of the neighboring minicolumns on the input of the interneuron in each minicolumn.

The overall synaptic activities of different cell populations in the ith minicolumn, $x_k^{(i)}(t)$, can be obtained from a convolution of the first-order kernel in (1) with the sum of all inputs as $p(t)$ by

$$x_k^{(i)}(t) = h(t) \otimes p(t) \tag{3}$$

where $\otimes$ is the convolution operator. According to the special shape of $h(t)$ in (1), the differential equation form of (3) is obtained by the following equation:

$$\ddot{x}_k^{(i)} = \frac{H}{\tau} p(t) - \frac{2}{\tau} \dot{x}_k^{(i)} - \frac{1}{\tau^2} x_k^{(i)}. \tag{4}$$

In the extended neural mass model, we consider a lattice form containing L minicolumns for the desired cortical area. The intercolumnar distance between minicolumns is D. The maximum permissible size of this lattice is limited by the available computational power only. Considering (4) for each $x_k^{(i)}(t)$ in Fig. 1, the activity of the ith minicolumn in the extended neural mass model is described by

$$\begin{aligned}
\ddot{x}_1^{(i)} &= \frac{H_e}{\tau_e}\left(u^{(i)} + \gamma_1 S\left(y^{(i)}\right) + G_S \sum_{j=1, j\neq i}^{L} a_{ij} S\left(y^{(j)}(t-\delta_{ij})\right)\right) \\
&\quad - \frac{2}{\tau_e}\dot{x}_1^{(i)} - \frac{1}{\tau_e^2} x_1^{(i)} \\
\ddot{x}_2^{(i)} &= \frac{H_e}{\tau_e}\left(\gamma_2 S\left(x_1^{(i)}\right) + G_P \sum_{j=1, j\neq i}^{L} b_{ij} S\left(y^{(j)}(t-\delta_{ij})\right)\right) \\
&\quad - \frac{2}{\tau_e}\dot{x}_2^{(i)} - \frac{1}{\tau_e^2} x_2^{(i)} \\
\ddot{x}_3^{(i)} &= \frac{H_i}{\tau_i}\gamma_4 S\left(x_4^{(i)}\right) - \frac{2}{\tau_i}\dot{x}_3^{(i)} - \frac{1}{\tau_i^2} x_3^{(i)} \\
\ddot{x}_4^{(i)} &= \frac{H_e}{\tau_e}\left(\gamma_3 S\left(y^{(i)}\right) + G_I \sum_{j=1, j\neq i}^{L} c_{ij} S\left(y^{(j)}(t-\delta_{ij})\right)\right) \\
&\quad - \frac{2}{\tau_e}\dot{x}_4^{(i)} - \frac{1}{\tau_e^2} x_4^{(i)} \\
u^{(i)}(t) &= e_i S\left(h_e(t) \otimes \mathrm{Stim}(t-\Delta_i)\right) + \eta(t) \\
y^{(i)} &= x_2^{(i)} - x_3^{(i)}
\end{aligned} \tag{5}$$

where $\otimes$ is convolution, $H_e = 3.25$ mV, $H_i = 29.3$ mV, $\tau_e = 10$ ms, $\tau_i = 15$ ms, $\gamma_1 = 50$, $\gamma_2 = 40$, $\gamma_3 = \gamma_4 = 12$, $e_0 = 2.5$, and $r = 0.56$e3 as given in [12]. $\delta_{ij} = \delta_c^* \mathrm{dist}(i,j)/D$ is the propagation delay between minicolumn i and minicolumn j where δ_c is the unit delay between two adjacent minicolumns. It is selected as 0.1 ms in our simulations, based on the physiological data. $\mathrm{dist}(i,j)$ is the Euclidean distance between the two minicolumns. Δ_i is the propagation delay between external stimulus ($\mathrm{Stim}(.)$) and the cortical columns. It is in the order of 40 ms as stated in [21]. $\eta(t)$ is physiological noise.

G_S, G_P, and G_I represent the influence of the neighboring minicolumns on the stellate cells, pyramidal cells and interneurons in a minicolumn. Due to similar structure of the minicolumns in an area, we assume that the G_S, G_P and G_I are fixed for all of the minicolumns in an area. a_{ij}, b_{ij} and c_{ij} represent the strength of the connections of different cell populations between the ith and the jth minicolumns. We use a Gaussian kernel for modeling the connections between minicolumns based on the physiological principle that the greater the distance between the two minicolumns, the weaker their influence on each other

$$a_{ij} = e^{-\frac{\mathrm{dist}(i,j)^2}{2\sigma_S^2}}; \quad b_{ij} = e^{-\frac{\mathrm{dist}(i,j)^2}{2\sigma_P^2}}; \quad c_{ij} = e^{-\frac{\mathrm{dist}(i,j)^2}{2\sigma_I^2}} \tag{6}$$

where $\sigma_S = \sigma_P = \sigma_I = 2^*D = 160$ μm as deduced from the data in [19]. e_i in (5) represents the strength of the afferent input to the ith minicolumn

$$e_i = e^{-\frac{\mathrm{dist}(i,m)^2}{2\sigma_E^2}} \tag{7}$$

where m is index of the minicolumn in the center of the area and $\sigma_E = 5^*D = 400$ μm as deduced from data in [19].

B. EEG and BOLD Signals in Proposed Integrated Model

The EEG is related to the $y^{(i)}(t)$ in (5) that shows the synaptic activations of the pyramidal cells. If we consider a vector along the vertical direction of the ith minicolumn whose absolute value is $y^{(i)}(t)$, the sum of the vectors in all minicolumns of an area constructs the equivalent current dipole (ECD) of the area. Since minicolumns are small compared to their distances to the EEG sensors and also the apical dendrites of the pyramidal cells are almost parallel, we assume that the minicolumns in an area are almost parallel. Thus, the algebraic sum of all $y^{(i)}(t)$ is enough for calculating the ECD in the area. The complete determination of the relationship between the ECD and the EEG requires the solution of the forward problem [23]. For simplicity in the simulations, we consider a homogenous head model and neglect the effect of the volume current, thus the sum of $y^{(i)}(t)$ is considered as the ERP or the EEG signal. It should be noted that finding the electric activation in a voxel from scalp potential by solving an inverse procedure is not the focus of this paper. In addition, note that it may be simplistic to state that an ECD is representative of an ERP or ERF and the neural activity presented by ECD is not necessarily coincident with the one that could be inferred from scalp data. However, this simplification does not affect the consistency of the model that relates the BOLD effect to the neural activity.

In the following, we introduce a relationship between the external stimulus and the BOLD signal in a single minicolumn. Then, using our extended neural mass model, we extend the idea to an area containing several minicolumns. The relationship between the stimulus and BOLD can be segregated into three separate steps: a step from the stimulus to the neural activity, another step from the neural activity to the CBF and a final step from the CBF to the BOLD. For the step from the CBF to the BOLD, Buxton *et al.* [10] have proposed the nonlinear Balloon model. For the step from the neural activity to the CBF, Friston *et al.* [18] have proposed a model of CBF autoregulation and added this relation to the model of Buxton in the EBM.

The relationship between the neural activity and CBF is assumed to be linear in EBM. However, it should be nonlinear, at least through a ceiling effect on CBF change [7], [24]. In our approach, we assume that the entire nonlinearity between the stimulus and CBF can be modeled by a nonlinear transformation from the stimulus to the neural activity as done in [24]. We use the EBM for relating the neural activity to the BOLD and introduce a new relationship between the stimulus and the neural activity.

In the neural mass model, ERP is only related to the synaptic activity of the pyramidal cells, but the neural activity as an index for increasing the CBF could be related to the activity of all cell types. The PSPs and action potentials (APs) are two main indices for showing the activity in a neuron. It is assumed that increasing the CBF is only related to the PSPs and there is no significant correlation between CBF and APs [25], [26]. Thus, neural activity should be related to the $x_1(t)$, $x_2(t)$, $x_3(t)$, and $x_4(t)$ in Fig. 1 which illustrate the overall synaptic activities of different neurons.

Considering the neural mass model for a single minicolumn, each $x_i(t)$ represents the activation of several synapses fired with different time lag δ_j

$$x_k(t) = \sum_j h_k(t - \delta_j); \quad k = 1,2,3,4 \tag{8}$$

where $h_k(.)$ is the same as that in (1). Based on the physiological principle that the neural activity and CBF are proportional to the consumed energy by the PSPs [26], [27], we propose the following representation for the neural activity $N(t)$ in a minicolumn:

$$N_k(t) \propto \sum_j I\left(h_k(t - \delta_j)\right) h_k(t - \delta_j); \quad k = 1,2,3,4 \tag{9}$$

where $I(h(t))$ is the current due to voltage $h(t)$ and the product of $I(h(t))$ by $h(t)$, according to the well-known circuit theory, shows the instantaneous power of the corresponding PSP. The $I(.)$ is generally a complex nonlinear function due to Hodgkin-Huxley equations. For simplicity, we consider a constant value for the synaptic current

$$N_k(t) \propto \sum_j h_k(t - \delta_j); \quad k = 1,2,3,4. \tag{10}$$

The total neural activity of the neurons considering (8) and (10) is, therefore

$$N(t) = \sum_{k=1}^{4} N_k(t) \propto \sum_{k=1}^{4} x_k(t). \tag{11}$$

Since $N(t)$ is some representation of the power consumed in an area, it is expected to have a positive value, as it is the case in [7] and [24]. In ERP regime of the Jansen's model, all $x_{\rm i}(t)$ are positive when the sigmoid function is positive. Since the sigmoid function in (2) is designed to produce a zero resting state for all variables, its value may become negative. Thus, we consider the absolute value of $x_{\rm i}(t)$ in our model to comply with the positivity of $N(t)$

$$N(t) \propto \sum_{k=1}^{4} |x_k(t)|. \tag{12}$$

We believe that both of the excitatory and inhibitory postsynaptic activities induce comparable increases in the neural activity and CBF. Hence, there are no differences between the inhibitory and excitatory PSPs in our model as illustrate in (12). This assumption is also used in a recent paper [7].

The neural activity in an area with L minicolumns is the sum of all neural activities in each minicolumn

$$N(t) \propto \sum_{i=1}^{L} \sum_{k=1}^{4} \left| x_k^{(i)}(t) \right| \tag{13}$$

where $x_k^{(i)}(t)$ for $k = 1, \ldots, 4$ are the overall synaptic activities of the ith minicolumn in the proposed extended neural mass model and can be calculated from (5). It should be noted that (13) can model event-related decrease of the BOLD signal, when it is used as the input of the EBM. This is due to the fact that the dynamics of the EBM can generate event-related decrease of the BOLD signal even with a positive input. As mentioned above, the extended neural mass model has the advantage of allowing a more accurate estimation of the EEG. There is a second advantage of the extended neural mass model in fMRI model. The summation in (13) is the image of a physiological principle: the energy consumed in a cortical area is the sum of the energies consumed by its minicolumns. Therefore, there is no approximation in this part of our computation for the neural activities. This is an advantage of considering numerous minicolumns in a cortical area instead of the simple Jansen model for the whole cortical area.

The neural activity computed in (13) is used as the input of the EBM from which the output BOLD signal is obtained. Instead of the proportionality (13), we consider its equality form, considering the proportional gain in the "neuronal efficacy ε" in the EBM. In the simulations, the constant parameters of the EBM are the same as those in [18]. The proposed integrated model in a cortical area contains the three sets of parameters as follows.

1) *Parameters of the Jansen's model*: the H_e, H_i, $\tau_{\rm e}$, $\tau_{\rm i}$, e_0, r, and γ are related to the Jansen's model, and because of the similarity of the minicolumns in an area, can be assumed fixed for all minicolumns in the area. We can reduce the redundancy by assuming $\gamma_2 = \gamma$, $\gamma_2 = 0.8^{*}\gamma$, and $\gamma_3 = \gamma_4 = 0.25^{*}\gamma$ based on the anatomical data [14].

2) *Parameters of the extended neural mass model*: they are σ_S, σ_P, σ_I, σ_E, G_S, G_P, G_I, δ_c, and Δ.

3) *Parameters of the EBM* according to the EBM in [18].

We are currently working on the estimation of these parameters using simultaneously acquired EEG and fMRI datasets. The results will be presented in the forthcoming paper.

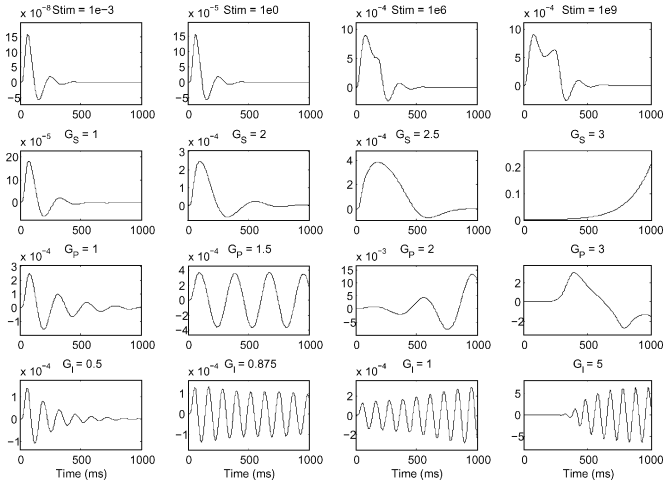

Fig. 2. Illustration of the capability of the proposed extended neural mass model for producing the ERPs. The stimulus is the Dirac delta function. The default value of the parameters in (5) are: $H_e = 3.25\,\mathrm{mV}$, $H_i = 29.3\,\mathrm{mV}$, $\tau_{\rm e} = 10\,\mathrm{ms}$, $\tau_{\rm i} = 15\,\mathrm{ms}$, $\gamma_1 = 50$, $\gamma_2 = 40$, $\gamma_3 = \gamma_4 = 12$, $e_0 = 2.5$, $r = 560$, $\delta_c = 0.1\,\mathrm{ms}$, $\Delta_i = 40\,\mathrm{ms}$, $\sigma_S = \sigma_P = \sigma_I = 2^{*}D = 160\,\mu\mathrm{m}$, and $\sigma_E = 5^{*}D = 400\,\mu\mathrm{m}$. In each subplot, all parameters are selected as the default values except for the parameters whose values are mentioned at the top of each subplot. Top row: effect of the external stimulus strength on ERP; $\sigma_E = 0$ in this simulation. Second row: effect of the stellate cells gain (G_S) on ERP. Third row: effect of the pyramidal cells gain (G_P) on ERP. Bottom row: effect of the inhibitory interneurons gain (G_I) on ERP.

III. Simulation Results

In this section, we illustrate simulation results of the extended neural mass model in a cortical area. The area contains $31 * 31 = 961$ minicolumns where intercolumnar distance is $D = 80\,\mu\mathrm{m}$. Minicolumns uniformly spread in a square area of $2.5 * 2.5\ \mathrm{mm}^2$. The Simulink toolbox of the MATLAB is used for solving (5) after converting it to a matrix state space form with $961 * 8 = 7688$ state variables. The solver type is "Fixed-step" with solver "Ode4 (Runge-Kutta)" and sample time is set as 0.1 ms. With this choice, due to the MATLAB approaches, the minimum possible propagation delay for solving the equations with solver Ode4 of MATLAB is 0.1 ms, which is what we chose for the unit propagation delay between minicolumns. In all simulations, the values of all parameters in (5) are as described in Section II unless stated otherwise.

A. ERP in Extended Neural Mass Model

The effects of the parameters of the extended neural mass model on ERP are illustrated in Fig. 2. The top row illustrates the saturations in thalamus relay nuclei and stellate cells to strong input stimuli. With weak input, the response is linear, leading to a linear relationship between the stimulus and peak ERP responses. However, with strong input, the neuronal activity leaves the linear domain of the sigmoid function in (2) and the shape of ERP changes due to the spiking saturation. The second row illustrates the effect of stellate cell's gain (G_S) to inputs from neighboring pyramidal cells. There is a shift on the positive and negative peaks of ERP when G_S increases. The peak times are N70/P200, N100/P330, and N180/P600 when G_S is 1, 2, and 2.5, respectively. The ERP will be unstable for large values of G_S. The third row illustrates the effect of G_P. The ERP tends to oscillate when G_P increases. Larger values

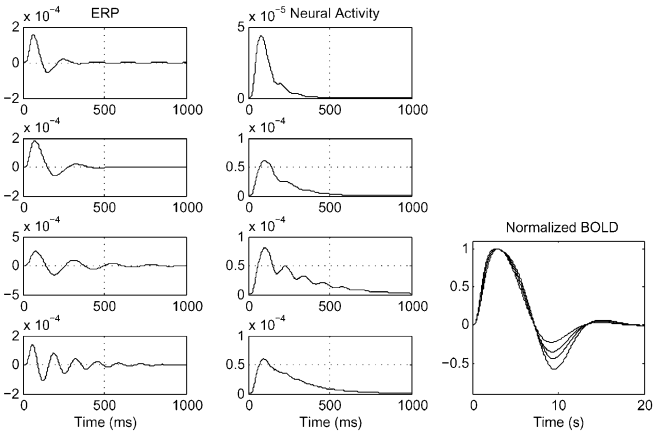

Fig. 3. Illustrations of the effects of the proposed integrated model parameters on the ERP, the neural activity and the BOLD signals. All conditions are similar to the left column in Fig. 2. The BOLD graphs correspond to the four subplots in the middle column, respectively, where moving from the top to the bottom subplots, their BOLD undershoots increase.

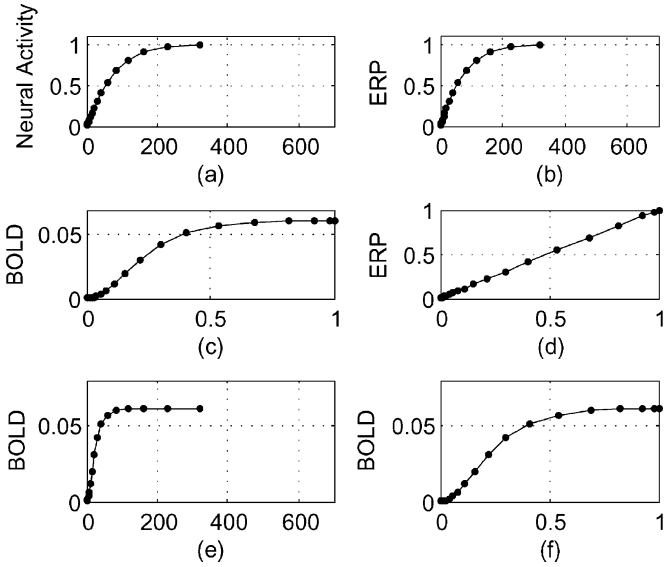

Fig. 4. Illustrations of the relationship between the external stimulus, the neural activity, the ERP and the BOLD in the proposed integrated model. The curves show the steady-state value of each variable when the stimulus input is the unit step function. Note that in Fig. 2, the stimulus is the Dirac delta function and the graphs show the time courses of the ERP, neural activity, and BOLD signal, respectively, whereas in this figure, the graphs show the steady-state value of these signals where the stimulus is the unit step function.

of G_P make ERP unstable. Very large values of G_P saturate the sigmoid functions of all pyramidal cells and produce saturated ERP's. The effect of the inhibitory interneuron's gain is illustrated in the bottom row of Fig. 2. Increasing the G_I causes more oscillation in the ERP. This is not surprising because the inhibitory interneurons with negative feedbacks are the main sources of oscillation in the Jansen's model.

B. ERP in Extended Neural Mass Model

Before dealing with the nonlinearities in the proposed integrated model, the sample waveform of the ERP, the neural activity and the BOLD responses to the impulse stimulus are illustrated in Fig. 3. The conditions generating the left column in Fig. 2 leads to the neural activities illustrated in the middle column of Fig. 3. The normalized BOLD responses for four different conditions are shown in the right side of Fig. 3. For this special case, the main difference between the BOLD responses is the peak values of the negative undershoot, as reported in the experimental results of [28], [29].

The relationships between the neural activity, BOLD and EEG signals for different strengths of the external stimulus are illustrated in Fig. 4. The input stimulus is the unit step function and the steady-state values of all variables are plotted in this figure. Fig. 4(a) and (b) summarizes a contribution of the paper. The relationship between the stimulus strength and the neural activity or the EEG signal is nonlinear. As mentioned before, the nonlinearity of our model is a result of the sigmoid function in (2).

When there is a strong stimulus, the sigmoid function of the output pulse rate of the thalamus relay nuclei and also the stellate cells saturate, thus the EEG and the neural activity saturate. With a weak input, the sigmoid function behaves linearly, thus the relationship is linear. There are several experimental results in the literature reporting a nonlinear relationship between the neural activity and the stimulus. For example, Jones and colleagues and also Nielsen and Lauritzen independently report that the relationship between the stimulus and the local field potential (as the neural activity) is like a sigmoid function [8], [9]. Surprisingly, their reported curve is quite similar to Fig. 4(a) supporting the approximations used for obtaining (12) in the proposed neural mass model.

Fig. 4(c) shows the saturated curve of the BOLD signal as a function of the neural activity, a direct consequence of the nonlinearity in the EBM. Both curves in Fig. 4(a) and (c) have saturation characteristics, thus the saturating relationship between the stimulus and the BOLD signal intensifies in Fig. 4(e). Fig. 4(d) illustrates that although both of the EEG and the neural activity saturate with strong stimulus, their relationship remains linear. It should be noted that the proportionality between the EEG steady-state values and the neural activity in Fig. 4(d) cannot be extended to their time series as shown in Fig. 3. The relationship between the EEG and fMRI signals is illustrated in Fig. 4(f). This relationship is linear for weak stimulus. With strong stimulus, due to the saturations in the Balloon model and the neural activity, the BOLD signal saturates faster than the EEG signal.

C. Synchronicity

The effects of synchronicity on the ERP and BOLD signals are illustrated in Fig. 5. For the simulation of the synchronicity in our model, the strength of the stimulus input to all minicolumns is set constant but the propagation delays between the stimulus and each of the minicolumns are set differently as:ms

$$\Delta_i = 40 \text{ ms} + \delta \frac{\text{dist}(i,m)}{D} \tag{14}$$

where Δ_i is the delay for the ith minicolumn (according to (5)) and m is the index of the central minicolumn in the center of the area, D is the unit intercolumn distance and δ is the unit delay.

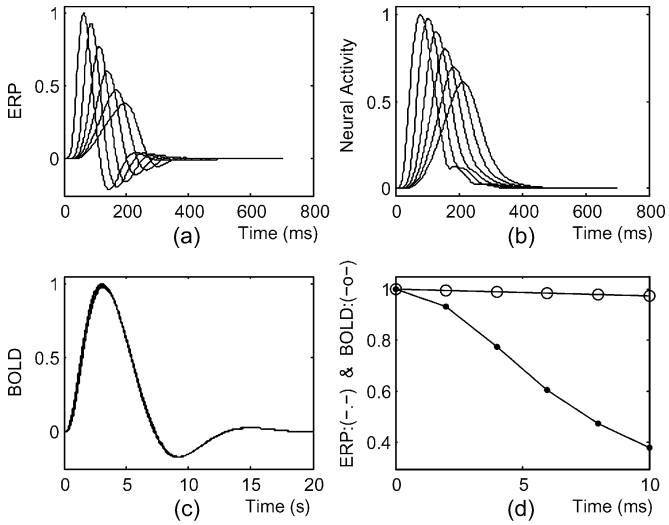

Fig. 5. Illustration of the synchronicity in the proposed model. Different delays [δ in (14)] between the stimulus and each of the minicolumns generate different waveforms for the ERP, the neural activity, and the BOLD in (a)–(c), respectively. The peak values of the ERP ($-.-$ plot) and BOLD ($-\circ-$ plot) signals for different delays are plotted in (d). The 6 curves in (a) and (b) correspond to different delays ($\delta = 0$, 2, 4, 6, 8, and 10 ms) where larger delays correspond to smaller peak values.

In this simulation, when two minicolumns are closer, their stimulus inputs have smaller time lag differences. The 6 curves in Fig. 5(a)–(c) are obtained using $\delta = 0$, 2, 4, 6, 8, and 10 ms, respectively. It should be noted that our goal here is to verify the effects of synchronicity in the production of the ERP and BOLD signals in the proposed model. However, we did not have access to the required experimental data to specifically evaluate physiological correspondence of the proposed synchronicity model.

The synchronicity between the minicolumns reduces as the delay δ increases, the electrical activities of the minicolumns cancel each other and the ERP reduces. Indeed, the simulation in Fig. 5(a) confirms that the ERP's peak reduces when the delay increases. On the other hands, the BOLD signal whose response time is in the order of 10 s is not sensitive to the delays in the order of ms. Fig. 5(c) and (d) illustrates that the BOLD signals for all 6 delays are quite similar. Although the delay causes the activities of the minicolumns occur at different times, but the overall neural activity and the total consumed energy do not change and hence the BOLD signals are similar. In Fig. 5(b), although the peaks of the neural activities reduce, the areas under the curves barely change. Again, this simulation supports the approximations used for obtaining (12) in the proposed neural mass model.

IV. Conclusion

For the first time, the neural mass model is used to propose a new integrated MEG/EEG and fMRI model in this paper. The external stimulus is the input of the model and simultaneous EEG and BOLD signals are the outputs of the model. In our method, we extend the classical neural mass model according to the physiological principles of the cortical minicolumns and their connections. The populations of different cells interact with themselves in a minicolumn and also receive inputs from the axons of the pyramidal cells in the neighboring minicolumns. Our simulations illustrate that the proposed extended neural mass model is capable of generating various types of ERP. Moreover, the extended neural mass model is the base of a new fMRI model. Indeed, it allows introducing a new nonlinear model of the neural activity. The resulting neural activity is used as the input of the extended Balloon model in order to generate the BOLD signal. Different applications could be foreseen for this new integrated model. It is possible that certain neurological diseases change the behavior of some minicolumns in a brain region. These behaviors are characterized in our model by the values of some parameters, which can be estimated using MEG/EEG and fMRI data. Thus, our model and its parameterization can help to diagnose or characterize the related neurological diseases. In addition, the proposed bottom-up model is instrumental in evaluating the upcoming top-down combined methods for simultaneous analysis of MEG/EEG and fMRI.

References

[1] A. M. Dale, A. K. Liu, and B. R. Fisch, "Dynamic statistical parametric mapping: combining fMRI and MEG for high-resolution imaging of cortical activity," *Neuron*, vol. 26, pp. 55–67, 2000.

[2] B. Horwitz and D. Poeppel, "How can EEG/MEG and fMRI/PET data be combined?," *Hum. Brain Mapp.*, vol. 17, pp. 1–3, 2002.

[3] A. K. Liu, J. W. Belliveau, and A. M. Dale, "Spatiotemporal imaging of human brain activity using functional MRI constrained magnetoencephalography data: Monte-Carlo simulations," *Proc. Nat. Acad. Sci. USA*, vol. 95, pp. 8945–8950, 1998.

[4] E. Martinez-Montes, P. A. Valdes-Sosa, F. Miwakeichi, R. I. Goldman, and M. S. Cohen, "Concurrent EEG/fMRI analysis by multiway partial least squares," *NeuroImage*, vol. 22, pp. 1023–1034, 2004.

[5] A. Babajani, M. H. Nekooei, and H. Soltanian-Zadeh, "Integrated MEG and fMRI model: synthesis and analysis," *Brain Topogr.*, vol. 18, no. 2, pp. 101–113, Dec. 2005.

[6] J. Riera, J. Bosch, O. Yamashita, R. Kawashima, N. Sadato, T. Okada, and T. Ozakic, "fMRI activation maps based on the NN-ARx model," *NeuroImage*, vol. 23, pp. 680–697, 2004.

[7] J. Riera, E. Aubert, K. Iwata, R. Kawashima, X. Wan, and T. Ozaki, "Fusing EEG and fMRI based on a bottom-up model: inferring activation and effective connectivity in neural masses," *Philosophical Trans.: Biol. Sci.*, vol. 360, no. 1457, pp. 1025–1041, 2005.

[8] M. Jones, N. Hewson-Stoate, J. Martindale, P. Redgrave, and J. Mayhew, "Nonlinear coupling of neural activity and CBF in rodent barrel cortex," *NeuroImage*, vol. 22, pp. 956–965, 2004.

[9] A. N. Nielsen and M. Lauritzen, "Coupling and uncoupling of activity-dependent increases of neuronal activity and blood flow in rat somatosensory cortex," *J. Physiol.*, vol. 533, pp. 773–785, 2001.

[10] R. B. Buxton, E. C. Wong, and L. R. Frank, "Dynamics of blood flow and oxygenation changes during brain activation: the balloon mode," *Magn. Reson. Med.*, vol. 39, pp. 855–864, 1998.

[11] O. David and K. J. Friston, "A neural mass model for MEG/EEG: coupling and neuronal dynamics," *NeuroImage*, vol. 20, pp. 1743–1755, 2003.

[12] O. David, L. Harrison, and K. J. Friston, "Modelling event-related responses in the brain," *NeuroImage*, vol. 25, no. 3, pp. 756–770, 2004.

[13] W. J. Freeman, "Models of the dynamics of neural populations," *Electroencephalogr. Clin. Neurophysiol. [Suppl.]*, vol. 34, pp. 9–18, 1978.

[14] B. H. Jansen and V. G. Rit, "Electroencephalogram and visual evoked potential generation in a mathematical model of coupled cortical columns," *Biol. Cybern.*, vol. 73, pp. 357–366, 1995.

[15] F. H. Lopes da Silva, A. Hoeks, H. Smits, and L. H. Zetterberg, "Model of brain rhythmic activity. The alpha-rhythm of the thalamus," *Kybernetik*, vol. 15, pp. 27–37, 1974.

[16] P. A. Robinson, C. J. Rennie, J. J. Wright, H. Bahramali, E. Gordon, and D. L. Rowe, "Prediction of electroencephalographic spectra from neurophysiology," *Phys. Rev. E*, vol. 63, pp. 1–18, 2001.

[17] P. L. Nunez, *Electric Fields of the Brain*. New York: Oxford Univ. Press, 1981.

[18] K. J. Friston, A. Mechelli, R. Turner, and C. J. Price, "Nonlinear responses in fMRI: the balloon model, volterra kernels, and other hemodynamics," *NeuroImage*, vol. 12, pp. 466–477, 2000.
[19] V. Mountcastle, "The columnar organization of the neocortex," *Brain*, vol. 120, pp. 701–722, 1997.
[20] D. Buxhoeveden and M. F. Casanova, "The minicolumn hypothesis in neuroscience: a review," *Brain*, vol. 125, pp. 935–951, 2002.
[21] C. J. Rennie, P. A. Robinson, and J. J. Wright, "Unified neurophysiological model of EEG spectra and evoked potentials," *Biol. Cybern.*, vol. 86, no. 6, pp. 457–471, 2002.
[22] G. Pfurtscheller and F. H. Lopes da Silva, "Event-related EEG/MEG synchronization and desynchronization: basic principles," *Clin. Neurophysiol.*, vol. 110, pp. 1842–1857, 1999.
[23] S. Baillet, J. C. Mosher, and R. M. Leahy, "Electromagnetic brain mapping," *IEEE Signal Process. Mag.*, vol. 18, no. 6, pp. 14–30, Nov. 2001.
[24] R. B. Buxton, K. Uludag, D. J. Dubowitz, and T. T. Liu, "Modeling the hemodynamic response to brain activation," *NeuroImage*, vol. 23, no. S1, pp. S220–S233, 2004.
[25] M. Lauritzen and L. Gold, "Brain function and neurophysiological correlates of signals used in functional neuroimaging," *J. Neurosci.*, vol. 23, pp. 3972–3980, 2003.
[26] N. K. Logothetis, "MR imaging in the non-human primate: studies of function and of dynamic connectivity," *Curr. Opin. Neurobiol.*, vol. 13, pp. 630–642, 2003.
[27] D. Attwell and C. Iadecola, "The neural basis of functional brain imaging signals," *Trends. Neurosci.*, vol. 25, pp. 621–625, 2002.
[28] V. C. Austin, A. M. Blamire, S. M. Grieve, M. J. O'Neill, P. Styles, P. M. Matthews, and N. R. Sibson, "Differences in the BOLD fMRI response to direct and indirect cortical stimulation in the rat," *Magn. Reson. Med.*, vol. 49, pp. 838–847, 2003.
[29] V. Van Meir, T. Boumans, G. De Groof, J. Van Audekerke, A. Smolders, P. Scheunders, J. Sijbers, M. Verhoye, J. Balthazart, and A. Van der Linden, "Spatiotemporal properties of the BOLD response in the songbirds auditory circuit during a variety of listening tasks," *NeuroImage*, vol. 25, pp. 1242–1255, 2005.

Abbas Babajani was born in Babolsar, Iran, in 1972. He received B.S. degree in electronic engineering with honors in 1995 and M.S. degree in biomedical engineering in 1998 from University of Tehran, Tehran, Iran. He is currently working towards the Ph.D. degree at University of Tehran.

His research interest is integrated analysis of functional neuroimaging methods and solution of inverse problem in MEG/EEG.

Hamid Soltanian-Zadeh (S'90–M'92–SM'00) was born in Yazd, Iran, in 1960. He received the B.S. and M.S. degrees in electrical engineering: electronics from the University of Tehran, Tehran, Iran, in 1986 and the M.S.E. and Ph.D. degrees in electrical engineering: systems and bioelectrical sciences from the University of Michigan, Ann Arbor, MI, in 1990 and 1992, respectively.

Since 1988, he has been with the Department of Radiology, Henry Ford Health System, Detroit, MI, where he is currently a Senior Staff Scientist. Since 1994, he has been with the Department of Electrical and Computer Engineering, the University of Tehran where he is currently a full Professor. He has active research collaboration with Wayne State University, Detroit, MI, and the Institute for studies in theoretical Physics and Mathematics (IPM), Tehran, Iran. His research interests include medical imaging, signal and image processing and analysis, pattern recognition, and neural networks. He has published over 380 papers in journals and conference records or as book chapters in these areas. He has served on the scientific committees of several international conferences and editorial boards of the scientific journals. He has also served on the study sections of the National Institutes of Health (NIH), National Science Foundation (NSF), and international funding agencies.